Hindawi
International Journal of Aerospace Engineering
Volume 2022, Article ID 7026823, 13 pages
https://doi.org/10.1155/2022/7026823

Research Article

Design and Analysis of Direct Abort Orbits in the Earth-Moon Transfer Phase of Crewed Lunar Exploration Missions

Lin Lu,[1,2] Haiyang Li,[1,2] Wanmeng Zhou,[3] Xinfeng Wu,[3] and Huiru Cui[4]

[1]*College of Aerospace Science and Engineering, National University of Defense Technology, Changsha 410073, China*
[2]*Hunan Key Laboratory of Intelligent Planning and Simulation for Aerospace Missions, Changsha 410073, China*
[3]*China Astronaut Research and Training Center, Beijing 100094, China*
[4]*College of Defense Engineering, Army Engineering University of PLA, Nanjing 210007, China*

Correspondence should be addressed to Haiyang Li; lihaiyang@nudt.edu.cn

Received 1 January 2022; Revised 11 February 2022; Accepted 3 March 2022; Published 19 March 2022

Academic Editor: Christian Circi

A direct abort orbit design method is presented for direct abort missions in the Earth-Moon transfer phase of crewed lunar exploration missions. First, according to the demand of an emergency rescue in the Earth-Moon transfer phase, two direct abort orbit schemes are introduced. Then, a serial orbit design method is proposed for a high-fidelity direct abort orbit. An analytical model is established for the calculation of initial values, and the optimization design is performed in the high-fidelity orbit model to determine a single-impulse abort orbit. A hybrid optimization design process is proposed to generate a two-impulse abort orbit. The results of simulation examples verify the validity and feasibility of the proposed direct abort orbit design method. Finally, extensive simulations are carried out to analyze the characteristics of abort impulse and abort return time and reveal the general rules of direct abort orbits. The research conclusions can provide a reference for the design of emergency rescue schemes in future crewed lunar exploration missions.

1. Introduction

The Moon is the first choice for humans to explore the mysteries of space, and it is also the most suitable transition station to enter deep space for expanding the living space of humans. The lunar exploration areas of the early American Apollo missions were mainly concentrated near the equator. However, due to the special location environment of the Moon's polar regions and the discovery of water ice [1, 2], humans are paying increasing attention to the middle and high latitudes of the Moon and regard them as hot spot areas for the next exploration, even considering the establishment of a lunar base in the future [3, 4]. At the beginning of the 21st century, the "Constellation Program" announced by the United States clearly stated the mission goals of "full global access" and "return anytime". In recent years, the "Artemis Project" to return to the Moon has been proposed [5], which has set off a worldwide upsurge of crewed lunar exploration [6–8]. With the successful implementation of the Chang′E-5 mission [9, 10], an increasing number of Chinese people also expect China to carry people to the Moon as soon as possible. Crewed lunar exploration is a complex and systematic engineering practice that demands high-technology and has high-risk. Ensuring the safety of astronauts is the primary factor considered in engineering design. In the process of mission implementation, if a crewed spacecraft fails and the safety of the astronauts is threatened, the astronauts can abort the mission at any time through a predesigned emergency rescue strategy and return to the Earth safely. Orbit design is an important part of the top-level design of space missions. Therefore, an emergency return orbit scheme is also a vital part of the emergency rescue strategy. The design and analysis of the emergency return orbit are of great significance to the design and implementation of the entire mission.

In the Earth-Moon transfer phase of crewed lunar exploration missions, a free return orbit with high safety can be generally adopted, and a crewed spacecraft can safely return to the Earth along the free return orbit without perilune injection [11]. At present, many scholars have studied the

free return orbit. Zhang et al. [12] proposed a fast prediction algorithm based on linear approximation for the design of free return orbit, which can effectively balance calculation accuracy and efficiency. He et al. [13] investigated an adaptive LEO-phase free-return orbit design method. Bao et al. [14] designed a two-segment free return orbit using pseudostate theory. Yim and Baoyin [15] designed free return orbits launching from lower-latitude launch sites and landing at high-latitude landing sites in a high-fidelity orbit model. Li et al. [16] established an analytical model of multi-segment free return orbits based on the patched-conic method. However, the accessible lunar surface region of a free return orbit is very limited, confined to near the Moon's equator and unable to support the exploration of lunar high-latitude regions [17, 18]. A hybrid orbit is composed of a free return orbit segment and a nonfree return orbit segment. Its accessible lunar surface region is not restricted, so it has been widely used [19, 20]. There are also some studies on the design and analysis of hybrid orbits. Bass [21] described the design and optimization of a hybrid orbit considering the constraints of mission abort but did not give a specific calculation model. Bai et al. [22] used a differential correction algorithm to describe the design process of a hybrid orbit. Based on the double two-body hypothesis, Huang et al. [23] analyzed the characteristics of a hybrid orbit, mainly including the characteristics of energy consumption and flight time. In addition, Peng [24] investigated the reachable domain characteristic of a hybrid orbit. However, a hybrid orbit has autonomous return ability for the free return orbit segment, and the other segment does not have the ability of autonomous return. Therefore, to ensure the safety of astronauts, during the engineering demonstration stage, the issue of abort return must be considered, and an abort orbit scheme must be designed in advance.

Scholars have performed much analysis and design work related to the abort issues of crewed lunar exploration missions. Hyle et al. [25] summarized the abort planning of crewed spacecraft during each flight phase of the Apollo missions. Baker [26] explored the abort issues of the Earth-Moon transfer phase and circumlunar phase. Kelley and Adornato [27] presented a method to select and determine a way station of an abort orbit in the circumlunar phase. Merrick and Callas [28] studied the abort orbit with the shortest time in the Earth-Moon transfer phase. These investigations play an important role in promoting early crewed lunar exploration missions, but they only describe some conclusions and do not give specific models and algorithms. Xi et al. [29] reviewed the issues related to the abort orbit in crewed lunar exploration missions. Based on the two-body problem model, Bond [30] estimated the velocity increment required for an abort during the Earth-Moon transfer phase. Huang et al. [31, 32] analyzed the characteristics of near Earth and near Moon abort orbits for crewed lunar exploration missions. Ocampo and Saudemont [33] established an initial calculation model of a multi-impulse trans-Earth abort orbit. Although these studies put forward some specific calculation models of an abort orbit, they all perform the design in a low-fidelity orbit model, and the calculation accuracy needs to be improved.

On the basis of the above research results, this paper mainly studies a direct abort orbit during the Earth-Moon transfer phase of crewed lunar exploration missions. The main contributions are as follows: On the one hand, a serial design method is proposed for high-fidelity direct abort orbits, which provides an effective tool for accurately determining two kinds of direct abort orbits. An analytical model of initial values calculation is established for a single-impulse abort orbit, while a hybrid optimization design process is proposed for a two-impulse abort orbit. On the other hand, the general rules of direct abort orbits are revealed, which provides a reference for engineering practice. By adopting the proposed design method of direct abort orbits, the characteristics of direct abort orbits are discussed, including the abort impulse characteristic and abort return time characteristic.

The structure of this paper is as follows. Section 2 describes the issue of a direct abort orbit in the Earth-Moon transfer phase of crewed lunar exploration missions. Section 3 proposes a design method for direct abort orbits and obtains high-fidelity solutions of two kinds of direct abort orbits. Section 4 verifies the validity and feasibility of the orbit design method using numerical simulations and analyzes the characteristics of the direct abort orbits. Some conclusions of this study are summarized in Section 5.

2. Statement of the Problem

To achieve the crewed lunar exploration mission goal of "full global access" given by the new era and effectively support scientific research in lunar middle- and high-latitude regions, this paper adopts a hybrid orbit which is adopted during the Earth-Moon transfer phase of crewed lunar exploration missions. It is necessary to consider the capability of safely returning to the Earth if a failure occurs at any time during flight to ensure the safety of the astronauts.

In this way, once a crewed spacecraft fails in the free return segment of a hybrid orbit, if the situation is not urgent, it can continue to fly along the free return orbit and finally return to the Earth safely. If the situation is quite urgent, the mission must be aborted directly and it can return to the Earth along the direct abort orbit. Once the crewed spacecraft fails in the nonfree return segment of the hybrid orbit before reaching the Moon, if the situation is not urgent, it can enter the free return orbit again through a maneuver and return to the Earth safely after circling the Moon. If the situation is urgent, the mission must be aborted directly and it can return to the Earth along the direct abort orbit. This paper studies a direct abort orbit in the Earth-Moon transfer phase and mainly focuses on the design and analysis of a direct abort orbit in the nonfree return segment of a hybrid orbit.

There are two main ways of direct abort in the Earth-Moon transfer phase, which are single-impulse abort and two-impulse abort, as shown in Figure 1. The process of a single-impulse abort is described as follows. After a crewed spacecraft fails, an abort impulse is applied at the abort point and the crewed spacecraft enters the single-impulse abort orbit. It reaches the reentry point after serval hours and

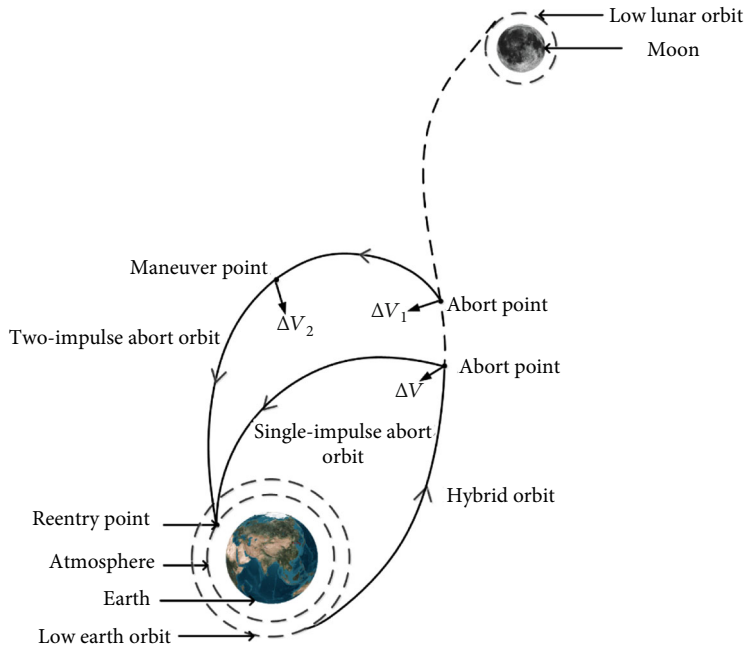

Figure 1: Diagram of direct abort orbits in the Earth-Moon transfer phase.

lands on the Earth's surface finally. The process of a two-impulse abort is depicted as follows. After a crewed spacecraft fails, a first abort impulse is applied at the abort point to enable the crewed spacecraft to enter the first segment of the two-impulse abort orbit. After serval hours, the crewed spacecraft reaches the maneuver point and applies a second abort impulse. Then, it reaches the reentry point along the second segment of the two-impulse abort orbit and lands on the Earth's surface finally.

3. Direct Abort Orbit Design Method

Aiming at a direct abort orbit in the Earth-Moon transfer phase of crewed lunar exploration missions, this section proposes an orbit design method from preliminary calculation to accurate design, which is used to design two kinds of direct abort orbits. For a single-impulse abort orbit, an analytical model is established for calculating the initial value, and the accurate design is performed in the high-fidelity orbit model. For a two-impulse abort orbit, a hybrid optimization design process is introduced to generate an accurate two-impulse abort orbit.

3.1. Preliminary Calculation. In the preliminary calculation stage, based on the two-body orbit assumption, preliminary calculation models are established for two kinds of direct abort orbits.

3.1.1. Preliminary Calculation Model of a Single-Impulse Abort Orbit. If the position vector $\mathbf{R}_0$ and the velocity vector $\mathbf{V}_0$ of the abort point are known, the flight-path angle before applying the abort impulse is calculated as

$$\Theta_{\mathrm{I}} = \arccos\left(\frac{h}{|\mathbf{R}_0| \cdot |\mathbf{V}_0|}\right), \tag{1}$$

where h is the magnitude of the orbital angular momentum.

The flight-path angle after applying the abort impulse is defined as

$$\Theta_{\mathrm{F}} = K_{\Theta} \cdot \Theta_{\mathrm{I}}, \tag{2}$$

where K_{Θ} is the ratio of the flight-path angle after applying the abort impulse to the flight-path angle before applying the abort impulse.

When the distance of the reentry point with respect to the Earth R_{Reen} and the flight-path angle of the reentry point Θ_{Reen} are given, according to the law of the conservation of angular momentum and the law of the conservation of energy, the following equation can be obtained:

$$\begin{cases} V_{\mathrm{Reen}}^2 = V_{\mathrm{F}}^2 + 2\mu_{\mathrm{e}}\left(\dfrac{1}{R_{\mathrm{Reen}}} - \dfrac{1}{R_{\mathrm{F}}}\right), \\ R_{\mathrm{F}} V_{\mathrm{F}} \cos\Theta_{\mathrm{F}} = R_{\mathrm{Reen}} V_{\mathrm{Reen}} \cos\Theta_{\mathrm{Reen}}, \end{cases} \tag{3}$$

where V_{Reen} is the velocity magnitude of the reentry point, V_{F} is the velocity magnitude after applying the abort impulse, μ_{e} is the gravitational parameter of the Earth, and R_{F} is the distance of the abort point with respect to the Earth after applying the abort impulse.

By rearranging Equation (3), the following equation is obtained:

$$V_F^2 = \frac{2\mu_e((1/R_{Reen}) - (1/R_F))}{\left(R_F^2 \cos^2\Theta_F / R_{Reen}^2 \cos^2\Theta_{Reen}\right) - 1}. \quad (4)$$

Assuming that the abort impulse does not change the orbital plane, in the local vertical local horizon (LVLH) coordinate system, the magnitude of the components of the abort impulse in each direction is given by

$$\begin{cases} \Delta V_{LVLHx} = V_F \sin\Theta_F - V_0 \sin\Theta_I, \\ \Delta V_{LVLHy} = V_F \cos\Theta_F - V_0 \cos\Theta_I, \\ \Delta V_{LVLHz} = 0. \end{cases} \quad (5)$$

Through coordinate system transformation, the abort impulse vector in the geocentric J2000 coordinate system is expressed as

$$\Delta \mathbf{V}_{EJ2} = \mathbf{M}_{LVLH}^{EJ2} \Delta \mathbf{V}_{LVLH}, \quad (6)$$

where $\Delta \mathbf{V}_{LVLH}$ is the abort impulse vector in the LVLH coordinate system and $\mathbf{M}_{LVLH}^{EJ2}$ is the transformation matrix from the LVLH coordinate system to the geocentric J2000 coordinate system at the abort point, which is described as

$$\mathbf{M}_{LVLH}^{EJ2} = \mathbf{M}_3(-\Omega_0)\mathbf{M}_1(-i_0)\mathbf{M}_3(-\omega_0 - \theta_0), \quad (7)$$

where Ω_0, i_0, ω_0, and θ_0 are the right ascension of the ascending node, orbital inclination, argument of perigee, and true anomaly of the hybrid orbit at the abort point, respectively. $\mathbf{M}_3$ and $\mathbf{M}_1$ are the rotation matrices that rotate a certain angle around the Z-axis and the X-axis, respectively.

Thus, the abort impulse vector can be computed, and then the orbital elements of the single-impulse abort orbit can be obtained. The true anomaly of the reentry point is expressed as

$$\theta_{Reen} = \begin{cases} 2\pi - \arccos\left(\frac{1}{e_{SAO}}\left(\frac{r_{pSAO}}{R_{Reen}}(1 + e_{SAO}) - 1\right)\right), & r_{pSAO} \le R_{Reen}, \\ 2\pi, & r_{pSAO} > R_{Reen}, \end{cases} \quad (8)$$

where e_{SAO} is the eccentricity of the single-impulse abort orbit and r_{pSAO} is the perigee radius of the single-impulse abort orbit.

The true anomaly of the abort point and the reentry point are determined, so the abort return time after the single-impulse abort is calculated by

$$T_{re} = \sqrt{\frac{a_{SAO}^3}{\mu_e}}[(E_{Reen} - e_{SAO}\sin E_{Reen}) - (E_{AP} - e_{SAO}\sin E_{AP})], \quad (9)$$

where E_{AP} and E_{Reen} are the eccentric anomalies of the abort point and the reentry point, respectively, which can be obtained by the corresponding true anomaly.

In summary, when the position vector $\mathbf{R}_0$ and the velocity vector $\mathbf{V}_0$ of the abort point are known, once K_Θ, the distance of the reentry point with respect to the Earth R_{Reen} and the flight-path angle of the reentry point Θ_{Reen} are given, the abort impulse and abort return time required for the single-impulse abort are determined, and then the single-impulse abort orbit can be preliminarily generated.

3.1.2. Preliminary Calculation Model of a Two-Impulse Abort Orbit. When the fuel of a crewed spacecraft is limited, in some cases, it is impossible to perform a single-impulse abort. In the case that a single-impulse abort cannot be carried out, a two-impulse abort can be adopted to optimize the total abort impulse and realize an abort return.

From the preliminary calculation model of a single-impulse abort orbit, it is known that if the position vector $\mathbf{R}_0$ and the velocity vector $\mathbf{V}_0$ of the abort point, the distance with respect to the Earth R_{Reen}, and the flight-path angle Θ_{Reen} of the reentry point are given and the ratio of the flight-path angle after applying the abort impulse to the flight-path angle before applying the abort impulse is denoted by $K_{\Theta 1}$, the first abort impulse can be obtained.

When the time interval between the two abort impulses is given, the eccentric anomaly E_{AP2} at the maneuver point can be calculated iteratively using the following equation:

$$T_{re1} = \sqrt{\frac{a_{TAO1}^3}{\mu_e}}[(E_{AP2} - e_{TAO1}E_{AP2}) - (E_{AP1} - e_{TAO1}E_{AP1})], \quad (10)$$

where e_{TAO1} is the eccentricity of the first segment of the two-impulse abort orbit after applying the first abort impulse and E_{AP1} is the eccentric anomaly of the abort point after applying the first abort impulse.

The true anomaly of the maneuver point is computed from the eccentric anomaly of this point, and then, the orbit elements at this point can be obtained. The position vector and velocity vector before applying the second abort impulse can be acquired through transformation. Assuming that the ratio of the flight-path angle after applying the second abort impulse to the flight-path angle before applying the second abort impulse is $K_{\Theta 2}$, the second abort impulse and flight time of the second segment of the two-impulse abort orbit are calculated by referring to the preliminary calculation model of the single-impulse abort orbit.

Thus, the two-impulse abort orbit design problem is transformed into a constrained nonlinear programming problem. The design variables include $K_{\Theta 1}$, T_{re1}, and $K_{\Theta 2}$. Once these design variables have been determined, a two-impulse abort orbit can be generated, which can be expressed as

$$\mathbf{Y}_{TAO} = f(K_{\Theta 1}, T_{re1}, K_{\Theta 2}). \quad (11)$$

The constraint conditions consider abort return time

and the reentry corridor constraints, that is,

$$\begin{cases} T_{\mathrm{re}} \le T_{\max}, \\ R_{\mathrm{Reen}} = R_{\mathrm{req}}, \\ \Theta_{\mathrm{Reen}} = \Theta_{\mathrm{req}}, \end{cases} \tag{12}$$

where $T_{\max}$ is the maximum abort return time allowed, R_{req} is the required distance of the reentry point with respect to the Earth, and Θ_{req} is the required flight-path angle of the reentry point.

In actual abort return missions, it is generally expected that the energy consumption is minimal in the two-impulse abort return process. In the preliminary calculation, the optimization objective function is set to be the minimum total abort impulse, that is,

$$J_{\mathrm{TAO0}} = (\Delta V)_{\min}, \tag{13}$$

where ΔV is the magnitude of the total abort impulse.

To solve this nonlinear programming problem, this study adopts the improved differential evolution algorithm DE_CMSBHS (Differential Evolution Algorithm with Combined Mutation Strategies and Boundary Handing Scheme). Based on the classical differential evolution algorithm framework, DE_CMSBHS introduces combined mutation strategies and combined boundary-handing schemes and adopts an adaptive parameter control method, which has better global search ability and optimization stability [34].

3.2. Accurate Design. During the accurate design stage, based on a high-fidelity orbit model, with the result of the preliminary calculation as the initial value, an accurate direct abort orbit is designed.

In the geocentric J2000 coordinate system, considering the relevant perturbation factors, the high-fidelity orbit model is described as

$$\frac{\mathrm{d}^2\mathbf{R}}{\mathrm{d}t^2} = -\frac{\mu_e \mathbf{R}}{R^3} + \mathbf{A}_{\mathrm{N}} + \mathbf{A}_{\mathrm{NSE}} + \mathbf{A}_{\mathrm{NSM}} + \mathbf{A}_{\mathrm{R}} + \mathbf{A}_{\mathrm{D}} + \mathbf{A}_{\mathrm{P}} \tag{14}$$

where $\mathbf{R}$ is the position vector of the spacecraft with respect to the geocentric J2000 coordinate system; $\mathbf{A}_{\mathrm{N}}$ is the gravitational perturbation of the N-body, where only the solar and lunar perturbations are considered and the relative positions between the stars are obtained from the JPL DE405 ephemeris; $\mathbf{A}_{\mathrm{NSE}}$ is the Earth nonspherical perturbation, here 6 degrees by 6 orders is adopted using the WGS84 model; $\mathbf{A}_{\mathrm{NSM}}$ is the Moon nonspherical perturbation, in which here 6 degrees by 6 orders is adopted using the LP165P model; $\mathbf{A}_{\mathrm{R}}$ is the solar radiation pressure perturbation that is related to the spacecraft area to mass ratio and the reflection factor; $\mathbf{A}_{\mathrm{D}}$ is the atmospheric drag perturbation; and $\mathbf{A}_{\mathrm{P}}$ is the thrust acceleration. The perturbations of Jupiter, Venus, and other large planets, the Earth tides, and the relativistic effect are ignored. The RKF78 integrator with variable pitch is selected as the integrator to perform the numerical integration.

3.2.1. Accurate Design Algorithm of a Single-Impulse Abort Orbit. In the accurate design of a single-impulse abort orbit, with the result of the preliminary calculation as the initial value, forward numerical integration is performed in the high-fidelity orbit model. The design variables are the abort impulse vector $\Delta\mathbf{V}_{\mathrm{EJ2}}$ and the abort return time T_{re}. After forward extrapolation in the high-fidelity orbit model, the state parameters of the reentry point can be obtained. The constraint condition is the constraint of the reentry corridor, that is, the constraints of the distance with respect to the Earth and the flight-path angle of the reentry point. To improve the convergence speed of the high-fidelity solution, the equality constraints are set as the objective function [35]:

$$J_{\mathrm{SAO}} = \sigma_1 \left| R'_{\mathrm{Reen}} - R_{\mathrm{req}} \right| + \sigma_2 \left| \Theta'_{\mathrm{Reen}} - \Theta_{\mathrm{req}} \right| \tag{15}$$

where σ_1 and σ_2 are weight factors and R'_{Reen} and Θ'_{Reen} are variation values of the distance with respect to the Earth and the flight-path angle of the reentry point in the iteration process, respectively.

The SQP_Snopt algorithm is adopted to optimize the single-impulse abort orbit. The SQP_Snopt algorithm is an advanced SQP algorithm [36], in which the finite quasi-Newton method is set to approximate the Hessian matrix of the Lagrange multiplier, thereby reducing the calculation of the Hessian matrix greatly and effectively improving the calculation speed. Hence, it is usually used to solve smooth nonlinear programming problems.

The single-impulse abort orbit design method from the preliminary calculation to the accurate design is shown in Figure 2.

3.2.2. Accurate Design Algorithm of a Two-Impulse Abort Orbit. In the accurate design of a two-impulse abort orbit, with the result of the preliminary calculation as the initial value, forward numerical integration is performed in the high-fidelity orbit model. The following variables are selected as the design variables: the first abort impulse vector $\Delta\mathbf{V}_{1\mathrm{EJ2}}$, the time interval between two abort impulses T_{re1}, the second abort impulse vector $\Delta\mathbf{V}_{2\mathrm{EJ2}}$, and the time interval between the maneuver point and the reentry point T_{re2}. After forward extrapolation in the high-fidelity orbit model, the state parameters of the reentry point can be obtained. The constraint condition is the constraint of the reentry corridor, that is, the constraints of the distance with respect to the Earth and the flight-path angle of the reentry point. The objective function is set to be the same as Equation (15).

The two-impulse abort orbit design method from the preliminary calculation to the accurate design is shown in Figure 3.

4. Simulation Verification

This section verifies the feasibility of the direct abort orbit design method proposed in this paper using numerical simulations and analyzes the characteristics of the direct abort orbit.

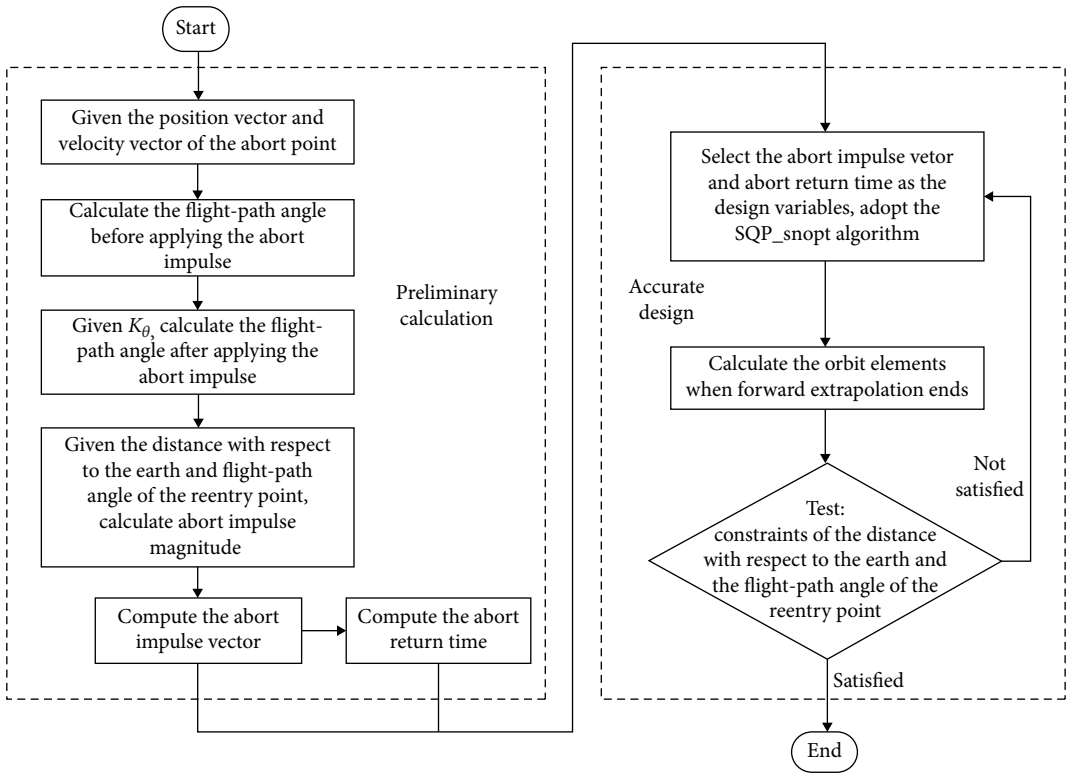

Figure 2: Flow chart of the single-impulse abort orbit design method.

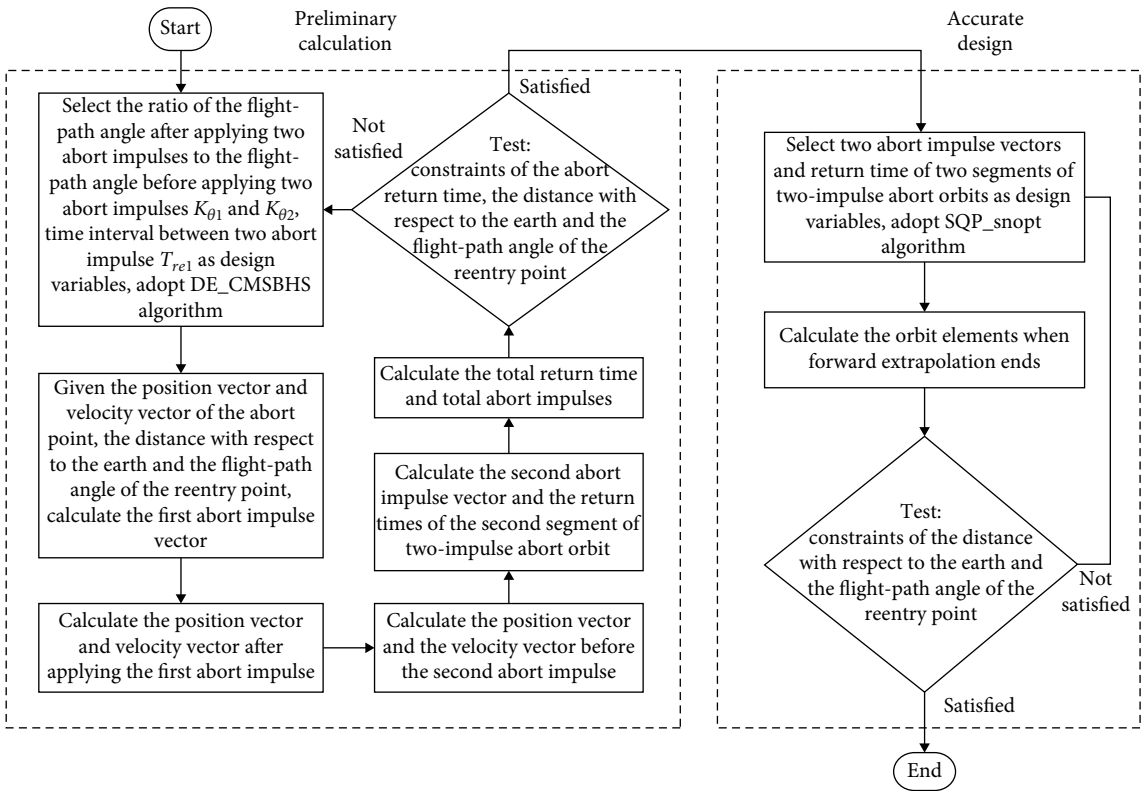

Figure 3: Flow chart of the two-impulse abort orbit design method.

Table 1: Orbital parameters of the hybrid orbit.

Parameter	Value
Departure time	2029-05-18 11:17:07.3131
Semimajor axis (km)	249547.1395
Eccentricity	0.9738
Orbital inclination (deg)	27.9922
Right ascension of the ascending node (deg)	143.7595
Argument of perigee (deg)	199.3091
True anomaly (deg)	28.4130
Hybrid maneuver time	2029-05-18 21:17:07.3131
Hybrid maneuver impulse vector (m/s)	(16.7923, 30.3731, -5.5991)

Table 2: The results of the single-impulse abort orbit (when K_Θ is 0.4).

Parameter	T (h)	$\Delta\mathbf{V}_{EJ2}$ (m/s)	ΔV (m/s)	T_{re} (h)
Preliminary calculation	4	(1263.92, -978.84, 19.71)	1598.75	35.21
Accurate design	4	(1264.82, -980.59, 20.12)	1600.54	35.21
Error		(0.90, -1.75, 0.41)	1.79	0.00
Preliminary calculation	8	(1159.82, -839.36, -8.37)	1431.71	43.72
Accurate design	8	(1161.75, -842.22, -7.72)	1434.94	43.72
Error		(1.93, -2.86, 0.65)	3.23	0.00
Preliminary calculation	12	(1073.05, -737.20, -25.48)	1302.13	51.83
Accurate design	12	(1076.54, -741.80, -25.18)	1307.60	51.83
Error		(3.49, -4.60, 0.30)	5.47	0.00

Table 3: The results of the single-impulse abort orbit (when K_Θ is 0.8).

Parameter	T (h)	$\Delta\mathbf{V}_{EJ2}$ (m/s)	ΔV (m/s)	T_{re} (h)
Preliminary calculation	4	(803.70, -629.91, 15.89)	1021.26	55.12
Accurate design	4	(804.02, -634.27, 17.43)	1024.23	55.12
Error		(0.32, -4.36, 1.54)	2.97	0.00
Preliminary calculation	8	(747.14, -547.12, -2.50)	926.05	66.08
Accurate design	8	(747.83, -554.93, -1.87)	931.24	66.08
Error		(0.69, -7.81, 0.63)	5.19	0.00
Preliminary calculation	12	(696.21, -484.11, -13.91)	848.09	76.27
Accurate design	12	(716.77, -471.00, 31.80)	858.26	76.27
Error		(20.56, 13.11, 45.71)	10.17	0.00

4.1. Simulation Example. First, a simulation example is used to examine the validity of the direct abort orbit design method. The simulation parameters are set as follows. A hybrid orbit is selected as the orbit of the Earth-Moon transfer phase for crewed lunar exploration missions, and the maneuver that transfers the spacecraft from the free return segment to the nonfree return segment is called the hybrid maneuver, which is performed 10 hours after departing the Earth. Table 1 provides the orbit parameters of the hybrid orbit. Referring to the analysis and statistics results of the Apollo missions [37], the reentry point altitude of the direct abort orbit is set to 122 km, and the flight-path angle of the reentry point is set to -6°.

4.1.1. Single-Impulse Abort Orbit Example. In the single-impulse abort case, it is assumed that an abort return occurs 4 hours, 8 hours, and 12 hours after the hybrid maneuver. When K_Θ is 0.4, by adopting the single-impulse abort orbit design method proposed in this paper, the single-impulse abort orbits in the three cases are calculated and the results of the preliminary calculation and accurate design are obtained as shown in Table 2. When K_Θ is 0.8, the results of the preliminary calculation and accurate design are obtained as shown in Table 3. In the tables, T is the time relative to the hybrid maneuver. $\Delta\mathbf{V}_{EJ2}$ is the abort impulse vector in the geocentric J2000 coordinate system. ΔV is the abort impulse magnitude.

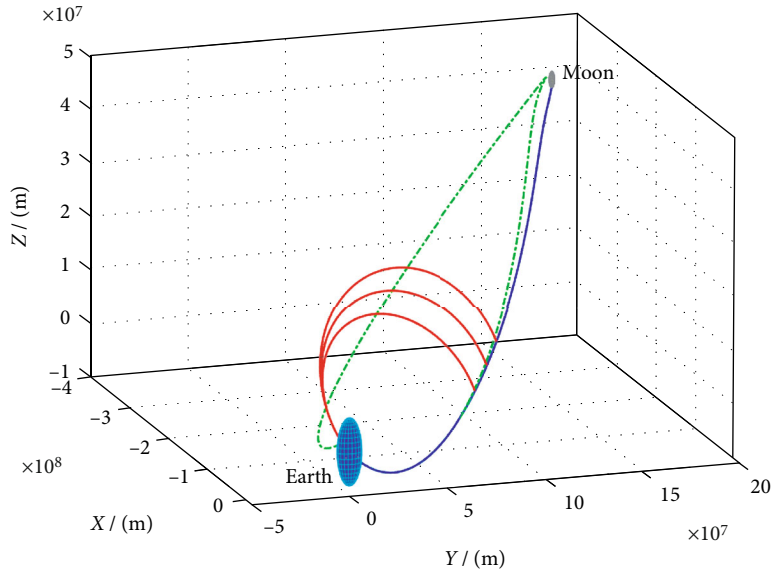

(a) Accurate single-impulse abort orbits in the three cases (when K_Θ is 0.4)

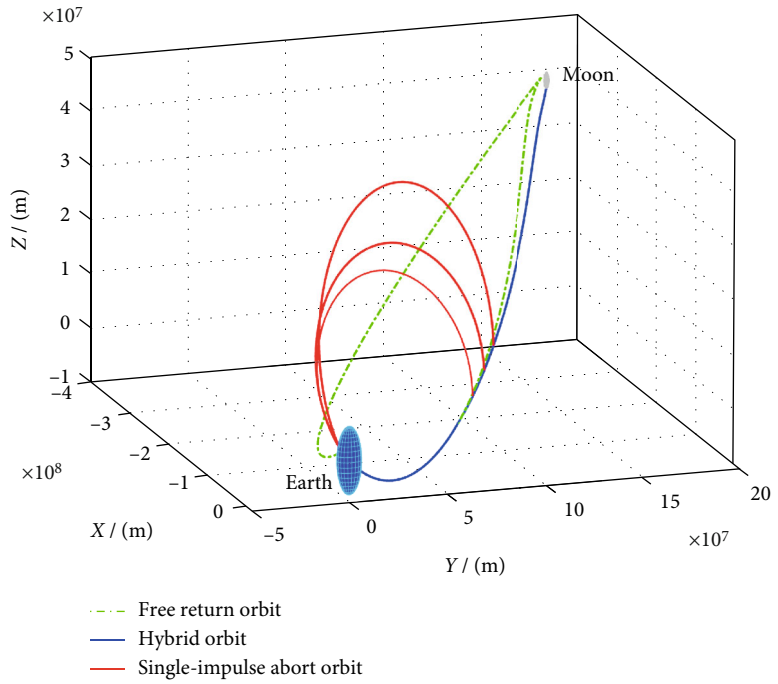

(b) Accurate single-impulse abort orbits in the three cases (when K_Θ is 0.8)

Figure 4: Accurate single-impulse abort orbits in the three cases of two simulation scenarios.

It can be seen from the tables that in the six cases, the results of the single-impulse abort orbit obtained from the preliminary calculation are close to those obtained from the accurate design. When K_Θ is 0.4, the accurate single-impulse abort orbits in the three cases are drawn in Figure 4(a). When K_Θ is 0.8, the accurate single-impulse abort orbits in the three cases are drawn in Figure 4(b). In the figure, the green orbit represents the free return orbit, the blue orbit represents the hybrid orbit, and the red orbits represent the single-impulse abort orbits of the three cases. Thus, the single-impulse abort orbit design method proposed in this paper can effectively generate a single-impulse abort orbit and the results of preliminary calculation can provide good initial values for accurate design.

4.1.2. Two-Impulse Abort Orbit Example. In the two-impulse abort case, it is assumed that the abort return occurs 4 hours, 8 hours, and 12 hours after the hybrid maneuver. The maximum abort return time is 1.5 times the minimum return time of a single-impulse abort orbit. By adopting the two-

Table 4: The results of the two-impulse abort orbits (when the maximum abort return time is 1.5 times the minimum return time of a single-impulse abort orbit).

Parameter	T (h)	$\Delta\mathbf{V}_{1EJ}$ (m/s)	ΔV_1 (m/s)	T_{re1} (h)	$\Delta\mathbf{V}_{2EJ}$ (m/s)	ΔV_2 (m/s)	ΔV (m/s)	T_{re} (h)
Preliminary calculation	4	(987.67, -769.25, 17.35)	1252.01	9.57	(23.41, -14.80, -1.13)	27.72	1279.73	44.56
Accurate design	4	(988.30, -770.57, 18.18)	1253.33	9.57	(23.55, -16.02, -0.62)	28.49	1281.82	44.56
Error		(0.63, -1.32, 0.83)	1.32	0.00	(0.14, -1.22, 0.51)	0.77	2.09	0.00
Preliminary calculation	8	(909.20, -661.83, -4.83)	1124.58	13.56	(2.45, -1.43, -0.17)	2.84	1127.42	55.15
Accurate design	8	(910.68, -664.02, -4.24)	1127.07	13.56	(2.86, -3.37, 1.82)	4.78	1131.85	55.15
Error		(1.48, -2.19, 0.59)	2.49	0.00	(0.41, -1.94, 1.99)	1.94	4.43	0.00
Preliminary calculation	12	(795.42, -550.75, -16.96)	967.63	1.93	(14.88, -9.77, -0.56)	17.81	985.44	67.00
Accurate design	12	(799.84, -565.67, -14.91)	979.77	1.93	(12.10, -3.33, -1.56)	12.64	992.41	67.00
Error		(4.32, -14.92, 2.05)	12.14	0.00	(-2.78, 6.44, -1.00)	-5.17	6.97	0.00

Table 5: The results of the two-impulse abort orbits (when the maximum abort return time is 1.25 times the minimum return time of a single-impulse abort orbit).

Parameter	T (h)	$\Delta\mathbf{V}_{1EJ}$ (m/s)	ΔV_1 (m/s)	T_{re1} (h)	$\Delta\mathbf{V}_{2EJ}$ (m/s)	ΔV_2 (m/s)	ΔV (m/s)	T_{re} (h)
Preliminary calculation	4	(1175.60, -911.82, 18.95)	1487.89	1.91	(31.14, -22.76, -0.12)	38.57	1526.46	37.03
Accurate design	4	(1175.85, -912.75, 19.39)	1488.67	1.91	(31.32, -23.67, 0.23)	39.25	1527.92	37.03
Error		(0.25, -0.93, 0.44)	0.78	0.00	(0.18, -0.91, 0.35)	0.68	1.46	0.00
Preliminary calculation	8	(1081.84, -784.20, -7.24)	1336.19	7.57	(0.51, -0.32, -0.02)	0.60	1336.79	46.76
Accurate design	8	(1082.84, -785.77, -5.82)	1337.91	7.57	(0.93, -1.75, 0.49)	2.04	1339.95	46.76
Error		(1.00, -1.57, 1.42)	1.72	0.00	(0.42, -1.43, 0.51)	1.44	3.16	0.00
Preliminary calculation	12	(987.37, -679.81, -22.79)	1198.98	7.87	(5.11, -3.13, -0.29)	6.00	1204.98	55.79
Accurate design	12	(988.97, -682.49, -22.06)	1201.81	7.87	(6.00, -5.58, 1.14)	8.28	1210.09	55.79
Error		(1.60, -2.68, 0.73)	2.83	0.00	(0.89, 2.45, 1.43)	2.28	5.11	0.00

impulse abort orbit design method proposed in this paper, the two-impulse abort orbits in the three cases are calculated and the results of the preliminary calculation and accurate design are obtained as described in Table 4. When the maximum abort return time is 1.25 times the minimum return time of a single-impulse abort orbit, the results of the preliminary calculation and accurate design are obtained as described in Table 5. In the tables, $\Delta\mathbf{V}_{1EJ}$ is the first abort impulse vector in the geocentric J2000 coordinate system. ΔV_1 is the magnitude of the first abort impulse. $\Delta\mathbf{V}_{2EJ}$ is the second abort impulse vector in the geocentric J2000 coordinate system. ΔV_2 is the magnitude of the second abort impulse.

It can be observed from the tables that in the six cases, the results of the two-impulse abort orbit obtained from the preliminary calculation are close to those obtained from the accurate design. When the maximum abort return time is 1.5 times the minimum return time of a single-impulse abort orbit, the accurate two-impulse abort orbits in these cases are shown in Figure 5(a). When the maximum abort return time is 1.25 times the minimum return time of a single-impulse abort orbit, the accurate two-impulse abort orbits in these cases are shown in Figure 5(b). In the figure, the green orbit represents the free return orbit, the blue orbit represents the hybrid orbit, the pink orbits represent the first segments of two-impulse abort orbits in the three cases, and the red orbits represent the second segments of two-impulse abort orbits in the three cases. Thus, the two-impulse abort orbit design method proposed in this paper can effectively determine the two-impulse abort orbit, and the results of preliminary calculation can provide a good initial value for accurate design.

4.2. Orbit Characteristic Analysis. During the engineering demonstration stage, the design of a specified direct abort orbit is not often given much attention, and much work is concentrated on grasping the relevant characteristics of this kind of orbit. Following the verification in the above subsection of the effectiveness and feasibility of the direct abort orbit design method proposed in this paper, this section adopts the method to perform extensive simulations and analyze the characteristics of the direct abort orbits.

4.2.1. Single-Impulse Abort Orbit Characteristic. First, the single-impulse abort orbit characteristics are analyzed. In terms of simulation parameters, the hybrid orbit parameters, the distance with respect to the Earth and the flight-path angle of the reentry point are consistent with those in Section 4.1. Figure 6 illustrates the curve of the required abort impulse changing with the abort time under different flight-path angle ratios. The figure indicates that the variation tendency of the required abort impulse is the same

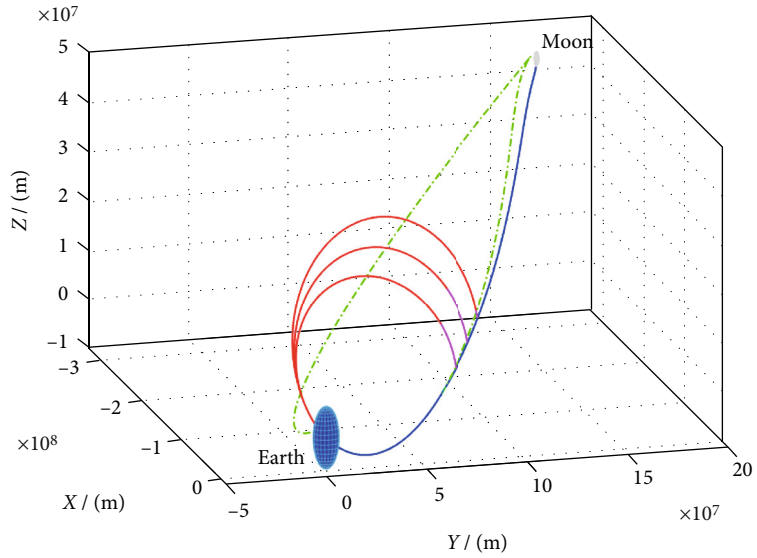

(a) Accurate two-impulse abort orbits in the three cases (when the maximum abort return time is 1.5 times the minimum return time of a single-impulse abort orbit)

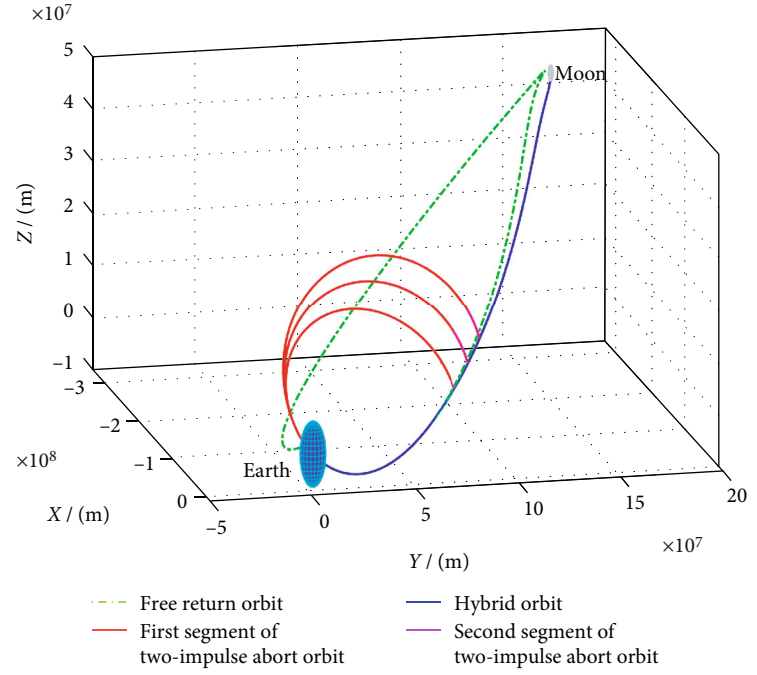

(b) Accurate two-impulse abort orbits in the three cases (when the maximum abort return time is 1.25 times the minimum return time of a single-impulse abort orbit)

Figure 5: Accurate two-impulse abort orbits in the three cases of two simulation scenarios.

and that the required abort impulse decreases with the delay of the abort time under different flight-path angles. In addition, compared to the flight-path angle before applying the abort impulse, the larger the variation of the flight-path angle after applying the abort impulse is, the larger the required abort impulse is.

Figure 7 presents the variation in the abort return time corresponding to the abort time in the cases of different flight-path angle ratios. The required abort return time has the same variation tendency in the cases of different flight-path angles. The change in the required abort return time corresponding to the abort time is approximately linear and increases with the delay of the abort time. In addition, the larger the change in flight-path angle after applying the abort impulse is, the smaller the required abort return time is. When the flight-path angle is 0, the required abort return time is the minimum. In this case, the single-impulse abort is regarded as the minimum return time abort.

4.2.2. Two-Impulse Abort Orbit Characteristic. Second, the two-impulse abort orbit characteristics are discussed. In terms of simulation parameters, the hybrid orbit parameters,

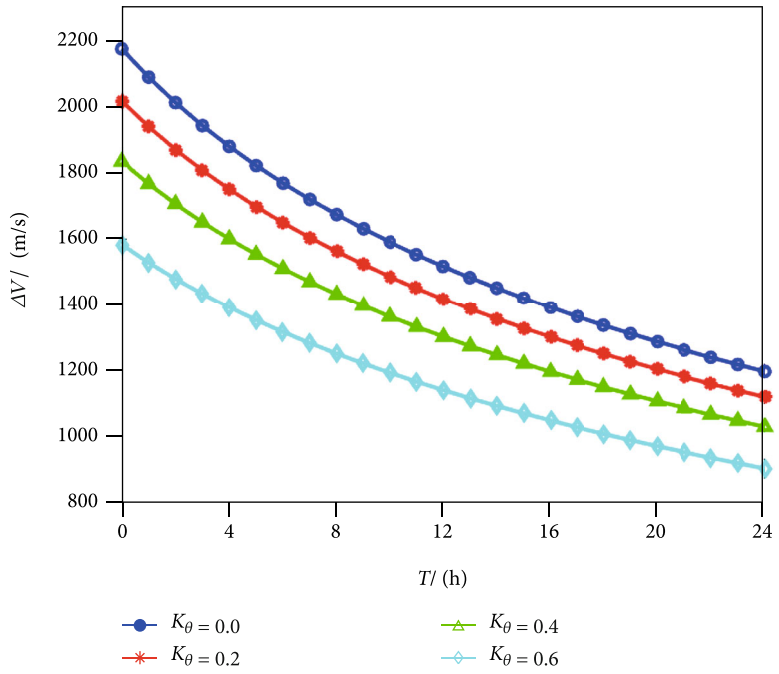

Figure 6: Abort impulse versus the abort time of the single-impulse abort orbit under different flight-path angle ratios.

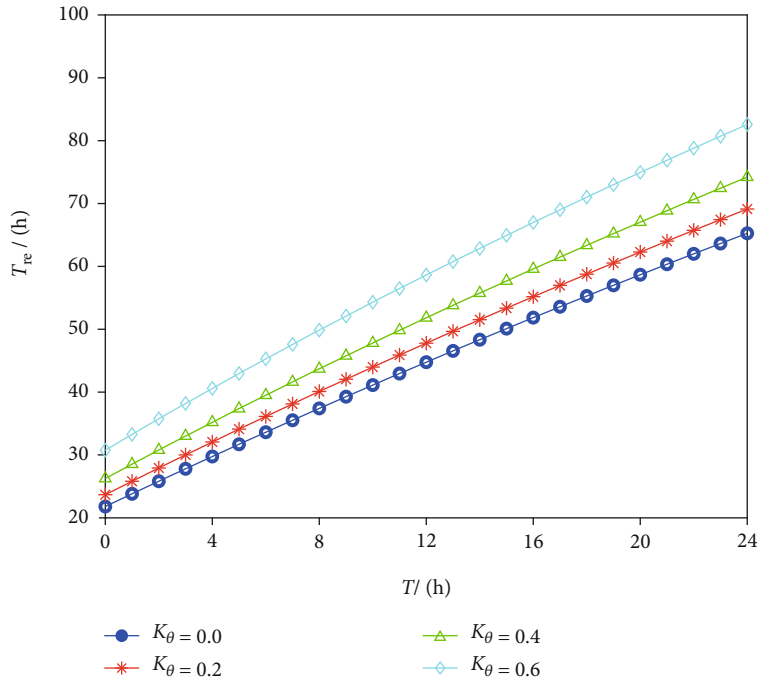

Figure 7: Abort return time versus the abort time of the single-impulse abort orbit under different flight-path angle ratios.

the distance with respect to the Earth, and the flight-path angle of the reentry point are consistent with those in Section 4.1. The variation in the total abort impulse is depicted in Figure 8 corresponding to the abort time in the cases of different maximum abort return time constraints. In the figure, K_{Tre} is the ratio of the maximum abort return time constraint to the minimum return time of the single-impulse abort. The required total abort impulse has the same variation tendency and decreases with the delay of the abort time. The larger the maximum abort return time constraint is, the smaller the required total abort impulse for two-impulse abort is. Compared with the single-impulse abort case of

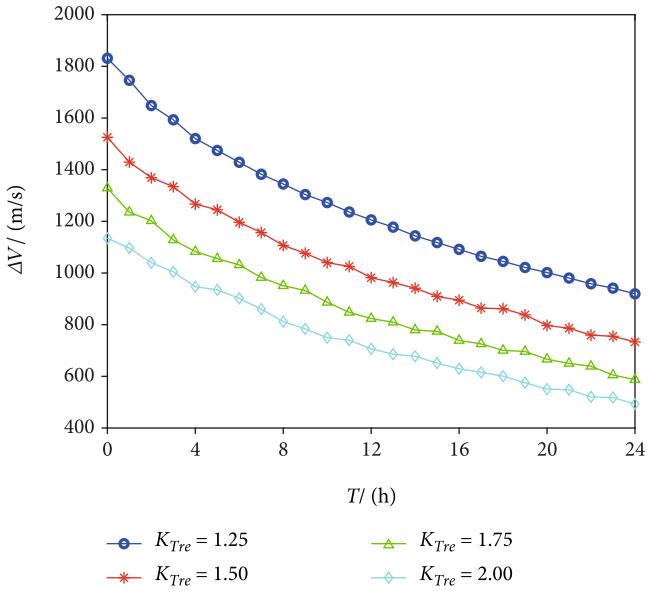

Figure 8: Total abort impulse versus the abort time of the two-impulse abort orbit under different maximum abort return time constraints.

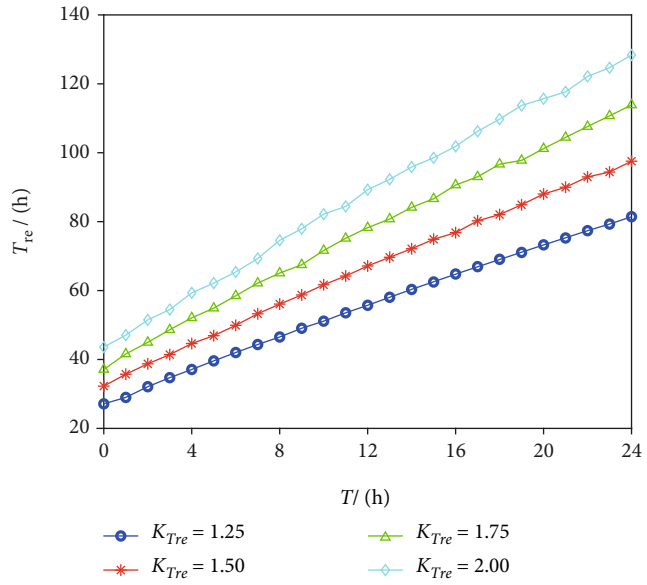

Figure 9: Abort return time versus the abort time of the two-impulse abort orbit under different maximum abort return time constraints.

the minimum abort return time, the required total abort impulse for the two-impulse abort is obviously reduced, which can save 350~1100 m/s.

Figure 9 depicts the variation in the required abort return time corresponding to the abort time in the cases of different maximum abort return time constraints. The change tendency of the required abort return time is similar under different maximum abort return time constraints. With the delay of the abort time, the required abort return time is increasing and changes approximately linearly. The larger the maximum abort return time constraint is, the longer the required abort return time is.

5. Conclusion

This paper proposes a direct abort orbit design method for direct abort missions in the Earth-Moon transfer phase of crewed lunar exploration. According to the requirement of emergency rescue in the Earth-Moon transfer phase, two kinds of direct abort orbit schemes are presented. A serial design method is adopted to generate a high-fidelity direct abort orbit. In terms of a single-impulse abort orbit, an analytical model is established for the initial value calculation, and the accurate solution is determined in the high-fidelity orbit model. In terms of a two-impulse abort orbit, a hybrid optimization design process is introduced, combining the DE_CMSBHS algorithm and the SQP_Snopt algorithm. The feasibility of this method is verified by the results of simulation examples. A number of simulation calculations adopting this method are performed to analyze the direct abort orbit characteristic. With the delay of the abort time, the required abort impulse gradually decreases, and the abort return time gradually increases. Compared to a single-impulse abort scheme, a two-impulse abort scheme can effectively reduce the fuel consumption and can reduce 350~1100 m/s. The research conclusions can provide an important reference for the design of a direct abort orbit scheme in the Earth-Moon transfer phase of future crewed lunar exploration missions.

Data Availability

The data used to support the findings of this study are included within the article.

Conflicts of Interest

The authors declare that there is no conflict of interest regarding the publication of this paper.

Acknowledgments

This work is supported by the National Natural Science Foundation of China (No. 12072365).

References

[1] S. Li, P. G. Lucey, R. E. Milliken et al., "Direct evidence of surface exposed water ice in the lunar polar regions," *Proceedings of the National Academy of Sciences of the United States of America*, vol. 115, no. 36, pp. 8907–8912, 2018.

[2] C. Zhu, P. B. Crandall, J. J. Gillis-Davis et al., "Untangling the formation and liberation of water in the lunar regolith," *Proceedings of the National Academy of Sciences of the United States of America*, vol. 116, no. 23, pp. 11165–11170, 2019.

[3] E. Detsis, O. Doule, and A. Ebrahimi, "Location selection and layout for LB10, a lunar base at the lunar north pole with a liquid mirror observatory," *Acta Astronautica*, vol. 85, pp. 61–72, 2013.

[4] J. L. Heldmann, A. Colaprete, R. C. Elphic et al., "Site selection and traverse planning to support a lunar polar rover mission: a case study at Haworth Crater," *Acta Astronautica*, vol. 127, pp. 308–320, 2016.

[5] V. Angelopoulos, "The Artemis mission," *Space Science Review*, vol. 165, no. 1-4, pp. 3–25, 2011.

[6] A. Zak, "Russia shoots for the moon," *Aerospace America*, vol. 53, no. 3, pp. 26–31, 2015.

[7] S. C. Aleina, N. Viola, R. Fusaro, G. Saccoccia, and V. Vercella, "Using the ESA exploration technology roadmaps in support of new mission concepts and technology prioritization," *Acta Astronautica*, vol. 154, pp. 170–176, 2019.

[8] K. J. Kim, "A research trend on lunar resources and lunar base," *The Journal of the Petrological Society of Korea*, vol. 26, no. 4, pp. 373–384, 2017.

[9] Y. Q. Qian, L. Xiao, J. W. Head, C. H. van der Bogert, H. Hiesinger, and L. Wilson, "Young lunar mare basalts in the Chang'e-5 sample return region, northern Oceanus Procellarum," *Earth and Planetary Science Letters*, vol. 555, article 116702, 2021.

[10] W. Yang and Y. T. Lin, "New lunar samples returned by Chang′e-5: opportunities for new discoveries and international collaboration," *The Innovation*, vol. 2, no. 1, article 100070, 2021.

[11] R. L. Berry, "Launch window and translunar orbit, lunar orbit, and trans-earth trajectory planning and control for the Apollo 11 lunar landing mission," in *AIAA 8th Aerospace Sciences Meeting*, New York, 1970.

[12] H. Zhang, Q. Luo, and C. Han, "Accurate and fast design algorithm for free-return lunar flyby trajectories," *Acta Astronautica*, vol. 102, pp. 14–26, 2014.

[13] B. Y. He, H. N. Li, and A. W. Zheng, "Adaptive LEO-phase free-return orbit design method for manned lunar mission based on LEO rendezvous," *The Journal of Astronautical Sciences*, vol. 66, no. 4, pp. 446–459, 2019.

[14] C. C. Bao, J. Y. Li, and H. X. Baoyin, "Two-segment lunar free-return trajectories design using the pseudostate theory," *Advances in Space Research*, vol. 61, no. 1, pp. 97–110, 2018.

[15] S. K. Yim and H. X. Baoyin, "High-latitude-landing circumlunar free return trajectory design," *Aircraft Engineering and Aerospace Technology*, vol. 87, no. 4, pp. 380–391, 2015.

[16] J. Y. Li, S. P. Gong, and H. X. Baoyin, "Generation of multisegment lunar free-return trajectories," *Journal of Guidance, Control, and Dynamics*, vol. 36, no. 3, pp. 765–775, 2013.

[17] B. Y. He, H. Y. Li, and J. P. Zhou, "Solution domain analysis of Earth-moon quasi-symmetric free-return orbits," *Transactions of the Japan Society for Aeronautical and Space Sciences*, vol. 60, no. 4, pp. 195–201, 2017.

[18] W. M. Zhou, H. Y. Li, B. Y. He, L. Yang, and Q. Peng, "Fixed-thrust Earth-moon free return orbit design based on a hybrid multi-conic method of pseudo-perilune parameters," *Acta Astronautica*, vol. 160, pp. 365–377, 2019.

[19] J. L. Goodman, "Apollo 13 guidance, navigation and control challenges," in *AIAA Space Conference and Exposition*, Pasadena, California, 2009.

[20] D. R. Adamo, "Apollo 13 trajectory reconstruction via state transition matrices," *Journal of Guidance, Control and Dynamics*, vol. 31, no. 6, pp. 1772–1781, 2008.

[21] R. A. Bass, "Optimization of hybrid trajectories for the Apollo mission under a DPS abort constraint," 1969, NASA-CR-103939.

[22] Y. Z. Bai, X. Q. Chen, and J. H. Li, "Free-return trajectory and hybrid trajectory design for manned lunar landing missions," *Journal of National University of Defense Technology*, vol. 32, no. 2, pp. 33–39, 2010.

[23] W. D. Huang, X. N. Xi, and W. Wang, "Characteristics analysis and design of hybrid trajectory for manned lunar landing mission based on double two-body model," *Journal of National University of Defense Technology*, vol. 32, no. 4, pp. 61–67, 2010.

[24] Q. B. Peng, *Optimal Trajectory Design and Characteristics Analysis for Manned Lunar Landing Mission with Emergency Capability [Ph.D. Thesis]*, National University of Defense Technology, Changsha, China, 2012.

[25] C. T. Hyle, C. E. Poggatt, and B. D. Weber, "Abort planning for Apollo missions," in *AIAA 8th Aerospace Sciences Meeting*, New York, 1970.

[26] M. K. Baker, "Apollo 15 translunar and lunar orbit aborts for the nominal launch-26 July 1971," 1971, NASA-CR-117347.

[27] T. Kelley and R. Adornato, "Determination of abort waystations on a nominal circumlunar trajectory," *Experimental Hematology*, vol. 32, no. 6, pp. 887–893, 1962.

[28] R. B. Merrick and G. P. Callas, "Prediction of velocity requirements for minimum time aborts from the midcourse region of a lunar mission," 1963, NASA-TN-D-1655.

[29] X. N. Xi, W. D. Huang, and W. Wang, "Review on abort trajectory for manned lunar landing mission," *Science China Technological Sciences*, vol. 41, no. 5, pp. 537–544, 2011.

[30] V. R. Bond, "A two-body analysis of deltaV requirements necessary for the abort from a translunar mission," 1964, NASA-TM-X-65061.

[31] W. D. Huang, X. N. Xi, and W. Wang, "Characteristic analysis of abort trajectory for manned lunar landing mission based on double two-body model," *Journal of Astronautics*, vol. 31, no. 9, pp. 2067–2074, 2010.

[32] W. D. Huang, X. N. Xi, and W. Wang, "Characteristic analysis and design of near moon abort trajectory for manned lunar landing mission," *SCIENCE CHINA Technological Sciences*, vol. 40, no. 12, pp. 1495–1502, 2010.

[33] C. Ocampo and R. R. Saudemont, "Initial trajectory model for a multi-maneuver moon-to-Earth abort sequence," *Journal of Guidance, Control, and Dynamics*, vol. 33, no. 4, pp. 1184–1194, 2010.

[34] Y. H. Zhu, Y. Z. Luo, and J. Zhang, "Packing programming of space station spacewalk events based on bin packing theory and differential evolution algorithm," in *2016 IEEE Congress on Evolutionary Computation*, pp. 877–884, Vancouver, Canada, 2016.

[35] B. Y. He, H. Y. Li, and J. P. Zhou, "Rapid design of circumlunar free return high accuracy trajectory and trans-lunar window for manned lunar landing mission," *Journal of Astronautics*, vol. 37, no. 5, pp. 521–528, 2016.

[36] E. G. Philip, W. Murray, and M. A. Saunders, "SNOPT: an SQP algorithm for large-scale constrained optimization," *SIAM Journal on Optimization*, vol. 12, no. 4, pp. 979–1006, 2002.

[37] C. A. Graves and J. C. Harpold, "Reentry targeting philosophy and flight results from Apollo 10 and 11," in *AIAA 8th Aerospace Science Meeting*, New York, 1970.